Nanostructure 3D metallic foams as electrocatalysts for electrooxidation and hydrolysis of sodium borohydride

Muhammed Kabir Bello
muhammed.k.bello@tecnico.ulisboa.pt
Instituto Superior Técnico, Universidade de Lisboa, Lisboa, Portugal

October 2017

Abstract

In a quest to enable dissemination of fuel cell technology, by reducing the cost factor and consequently reducing reliance on traditional fossil fuels, research efforts aim at exploring the catalytic activity of cheap and readily available non-noble metals like nickel, copper, iron, and cobalt in the form of nanoporous three-dimensional metallic foams towards electrooxidation of alternative fuels like sodium borohydride ($NaBH_4$) in direct borohydride fuel cells, and for its hydrolysis for H_2 generation and use in indirect fuel cells. The foams are deposited on a stainless-steel substrate, using the dynamic hydrogen bubble template, a simple electrodeposition technique. SEM/EDS is used to characterize the foams. Electrochemical testing of the foams in 0.03 M $NaBH_4$ in 2 M NaOH solutions revealed optimal performance of bi- and tri-metallic nickel, copper, and iron foams in electrooxidation, while cobalt based foams were superior for $NaBH_4$ hydrolysis.

Keywords: Sodium borohydride; dynamic hydrogen bubble template; electrocatalysis; nanostructured metallic foams.

1 Introduction

Fuel cells are electrochemical energy devices that convert chemical energy to electricity as long as they are supplied with a fuel and an oxidant. They offer the merits of a heat engine and a battery and eliminate the major drawbacks of both. First conceived in the 19th century by Sir William Grove, the technology recorded early successes in America's space program, but suffered a decline in interest as the era of global boom of fossil based fuel came upon us. Climatic consequences of anthropogenic dependence on fuel combustion technologies have spurred rekindling interests in fuel cells since the 20th century.

Amongst low temperature fuel cells, polymer electrolyte fuel cells, which typically operate at 80 ºC, have enjoyed reputation as more promising for residential and portable applications due to their characteristically high-power density. However, its large-scale development has met impediments from cost competitiveness to engineering design and safety concerns for hydrogen fueled devices [1]. The plausibility of a high specific energy liquid fuel considerably reduces the impediments earlier stated. To this effect, interest in

application of methanol as a fuel has been on the rise. Met with challenges that include the methanol crossover between electrodes, slower reaction kinetics and low open circuit potential, alternative fuels like sodium borohydride ($NaBH_4$) using the dissolved fuel principle hold the potential to mitigate the identified issues [2].

The earliest demonstration of direct borohydride fuel cells (DBFCs) was in the 1960's. DBFCs show superior performance to its methanol counterpart in capacity value, electrochemical activity, theoretical open circuit voltage (1.64 V against 1.21 V), fuel efficiency, and power performance at ambient operating temperature. These breakthroughs have intensified research efforts directed towards optimizing its performance [3,4]. $NaBH_4$ has a capacity of 5.67 Ahg^{-1} and hydrogen content of 10.6 wt.%. It hydrolyzes spontaneously in acidic medium, but is stable in alkaline medium, and thus is regarded an alkaline fuel [5]. Eq. 1 generally gives the oxidation of borohydride in aqueous alkaline medium. The alkaline electrolyte, characterized by low corrosion activity, allows for the possibility of using cheap and readily available non-precious metals as anode catalysts. However, this is both a pro and a con as most metals and their compounds, often catalyze the parallel occurring borohydride hydrolysis reaction (Eq. 2), giving rise to the challenge in the choice of anode electro catalyst for the cell [3].

$$BH_4^- + 8OH^- \rightarrow BO_2^- + 6H_2O + 8e^- \quad (E^0 = -1.24V \text{ vs. SHE}) \quad (1)$$

$$BH_4^- + 2H_2O \rightarrow BO_2^- + 4H_2 \quad (2)$$

2 Experimental

2.1 Substrate preparation

Electrodeposition was carried out in AISI 304 stainless steel substrates. Prior to deposition, the substrates were prepared with the following steps: (i) Polishing with LaboPol-25 machine with P600 silica carbide abrasive paper under flowing water; (ii) The substrates were then soaked in acetone and placed in an ultrasonic machine for 3 min to degrease the surface; (iii) the substrates were then air dried and weighed.

2.2 Foams electrodeposition

All reagents used were of analytical grade. Solutions were prepared with Millipore water according to standard procedure, using the molar concentrations shown in Table 1. In addition, 1.5 M H_2SO_4 and 1 M HCl were added to solution I to V. Electrodeposition was carried out in a two-electrode cell connected to a power source (Kikusui Electronics, Model PAB 32-3), with a platinum plate serving as counter electrode. The co-deposition of the metals was achieved in galvanostatic mode over 1.55 cm^2 area of the substrate at 3 A for 180 s for solutions I-V [14], while solution VI-VII were at 1 A cm^{-2} for 90 s, solution VIII was at 1 A cm^{-2} for 180 s. Each electrode was thoroughly rinsed with Millipore water, dried with a jet of air, weighed and stored in airtight plastic vials.

Table 1: Composition of the prepared electrodeposition solutions (in M).

Solution ID	$NiSO_4.6H_2O$	$CuSO_4.5H_2O$	$(NH_4)_2Fe(SO_4)_2.6H_2O$	NH_4Cl	$CoCl_2$	NaCl	$NiCl_2$
I	0.5	0.01	-	-	-	-	-
II	0.5	0.02	-	-	-	-	-
III	0.25	0.01	-	-	-	-	-
IV	0.1875	0.0075	0.375	-	-	-	-
V	0.01	0.005	0.25	-	-	-	-
VI	-	-	-	2	0.1	-	-
VII	-	-	-	1.5	0.03	0.05	0.07
		$CoSO_4.7H_2O$			H_3BO_3		
VIII	0.09	0.053	0.03	0.28	0.4	-	-

2.3 Foams characterization

Morphology and composition of the metallic foams were evaluated by scanning electron microscopy (SEM, Hitachi S2400) and energy dispersive X-ray spectroscopy (EDS, Rontec standard detector), respectively.

2.4 Electrochemical analysis

Electrochemical studies were carried out using a PAR 273A potentiostat (Princeton Applied Research, Inc.) connected to a dedicated computer with PowerSuite software installed. Using a three-electrode cell with a platinum mesh (Johnson Matthey) and a saturated calomel electrode (SCE) from Hanna instruments, as counter and reference electrodes, respectively. Hence, all potentials recorded in this study are relative to SCE reference. Cyclic voltammetry was used to study the irreversible oxidation of $NaBH_4$. By analyzing the variation of peak position as a function of scan rate, it is possible to gain information on the estimate of the anodic charge transfer coefficient, α. At the same time, the analysis of the peak current change with the electrode scan rate allows determination of the number of exchanged electrons, n.

2.5 Borohydride hydrolysis

The amount of generated hydrogen was measured by using MilliGascounter (Ritter). In a typical measurement, a 15mL solution containing 5 wt.% $NaBH_4$ and 0.4 wt.% NaOH is placed in an airtight flask fitted with an outlet for collection of produced H_2 gas, connected with the digital gas flow meter. The foam is placed in the solution at 60 °C to initiate hydrolysis reaction of sodium borohydride.

3 Results and discussion

3.1 Deposition of the metallic foams

Table 2 shows the composition of the deposited foams and their masses. Two samples were prepared for each foam composition, with both foam samples presenting relatively constant mass.

Table 2: Mass of foam catalysts deposited from electrodeposition solution.

Solution ID	Foam composition (from EDS)	Mass of catalyst / g	
I	$Ni_{52}Cu_{31}O_{17}$	0.0113	0.0143
II	$Ni_{34}Cu_{37}$	0.019	0.0178
III	$Ni_{36}Cu_{46}O_{18}$	0.009	0.0085
IV	$Ni_{14}Cu_{28}Fe_{41}O_{18}$	0.0097	0.0102
V	$Ni_4Cu_{48}Fe_{30}O_{12}$	0.0015	0.0023
VI	Co_{100}	0.0198	0.0195
VII	$Ni_{65}Co_{35}$	0.0253	0.025
VIII	$Ni_{62}Co_{24}Fe_{14}$	0.0129	0.0245

3.2 Morphological characterization

SEM, as shown in Figure 1, characterized the morphology of the metallic foams. High cathodic current densities employed during electrodeposition resulted in continuous bubbling of H_2, which limited the free volume

available for metal growth by blocking the transfer of active species, giving rise to three dimensional foam-like morphologies with randomly distributed micrometric and nanometric pores, obtained under mass transfer conditions [18].

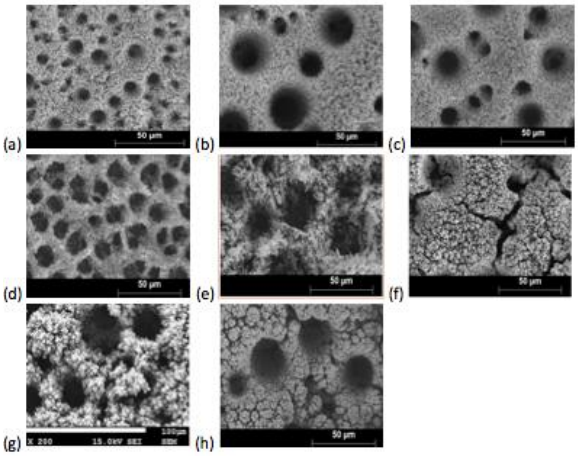

Figure 1: SEM images for the catalysts (a) $Ni_{52}Cu_{31}O_{17}$ (b) $Ni_{34}Cu_{37}$ (c) $Ni_{36}Cu_{46}O_{16}$ (d) $Ni_{14}Cu_{26}Fe_{41}O_{18}$ (e) $Ni_4Cu_{48}Fe_{30}O_{12}$ (f) Co_{100} (g) $Ni_{65}Co_{35}$ (h) $Ni_{62}Co_{24}Fe_{14}$.

It can be noticed that as nickel fractional composition is reduced in comparison to copper in the Ni-Cu binary foams, the circular definition of the porous structures is enhanced, the dendrites that characterize the pore walls are less ramified, increments in pore size is apparent and surface pore density is reduced. However, total porosity of three-dimensional foams does not depend only on the apparent pore size or surface pore densities but the voids resulting from the ferny-like structure. For ternary Ni-Cu-Fe foams, the introduction of iron seems to improve the interconnectivity of the pores and enhanced pore density. No clear pattern is observed in the distribution of pores on the cobalt foam, when compared with the earlier discussed foams. Cobalt foam's pore structures are crater shaped, with less voids in the pore walls. These characteristics are improved when co-deposited with nickel, as shown in Fig. 1g, except for the pore walls, which are more apparently cauliflower like. The introduction of iron to obtain ternary metallic foam of Co-Ni-Fe resulted in lumpy over growths and seemed to reduce the interconnectivity of pores.

3.3 Voltammetric studies and peak analysis

Previous investigation on the electrochemical behavior of Ni-Cu foams, found their voltammograms depictive of pseudocapacitive behavior (i.e., storing charge from reversible redox reactions, couple redox peaks in the potential range of -0.2 to 0.8 V were observed. The anodic peak corresponds to the oxidation of nickel and the cathodic peak to the corresponding reduction [18].

The mechanism of BOR at Ni based electrodes is still considerably inconclusive; therefore, making the peak assignment from voltammetric studies an arduous task. Tsionskii et al. suggested that BH_4^- is electrochemically inactive at Ni electrodes in the region between 0 and 0.6 V, hence anodic currents seen in that region stem from the oxidation of adsorbed H atoms from BH_4^- hydrolysis.

Figure 2 shows the effect of the potential scan rate in the borohydride oxidation CVs at each of the eight prepared foams. As expected, current densities increase with the scan rate, with the peak potential being progressively shifted to more positive potentials.

Shifts in peak potential, E_p, with the scan rate, ν, for BOR is described by Eq. 3, assuming it occurs as a single-step irreversible process,

$$E_p = E^0 + \frac{RT}{(1-\alpha)n_a F}\left[0.78 + \ln\left(\frac{D^{\frac{1}{2}}}{k_s}\right) + \ln\left(\frac{(1-\alpha)n_a F v}{RT}\right)^{\frac{1}{2}}\right] \quad (3)$$

Where E^0 is the formal potential (V), R is the universal gas constant (8.314 $JK^{-1}mol^{-1}$), T is the temperature (K), α is the charge transfer coefficient, n_a is the number of electrons involved in the rate determining step, F is the Faraday constant (96485 C mol^{-1}), D is the diffusion coefficient of BH_4^- (cm^2s^{-1}), and k_s is the standard heterogeneous rate constant (cm s^{-1}).

The fraction of energy that goes to anodic oxidation reaction, termed the charge transfer coefficient, α, is dependent on the reaction involved and the electrode material. D, the diffusion coefficient of BH_4^- is determined from Eq. 4, valid for 2 M NaOH solutions [21].

$$D = 5.57 \times 10^{-3} exp\left(\frac{-15.2 \times 10^3}{RT}\right) \quad (4)$$

The variation of peak current density j_p with scan rate v can be described by the Randles-Sevcik equation for irreversible processes (Eq. 5),

$$j_p = 2.99 \times 10^5 [(1-\alpha)n_a]^{\frac{1}{2}} nCD^{\frac{1}{2}}v^{\frac{1}{2}} \quad (5)$$

Where C is $NaBH_4$ bulk concentration in mol cm^{-3}, and all other symbols retain their definition.

Applying Eqs. 3 and 5 to the borohydride oxidation peaks shown in Figure 2 it is possible to calculate α and n, respectively. The kinetic data obtained from the peak analysis is summarized in Table 3.

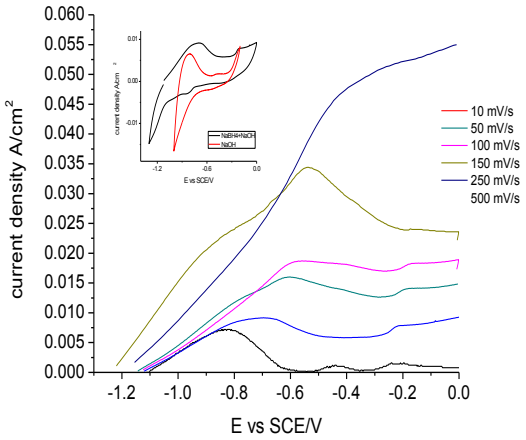

(a)

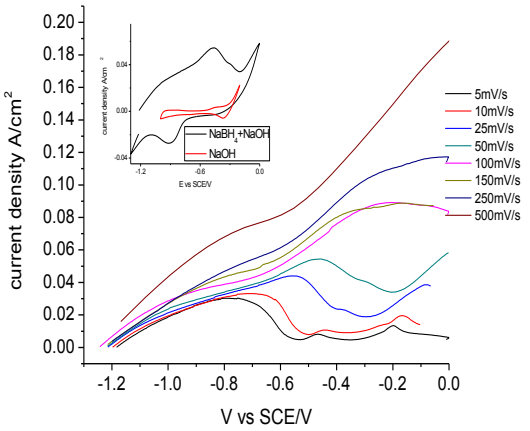

(b)

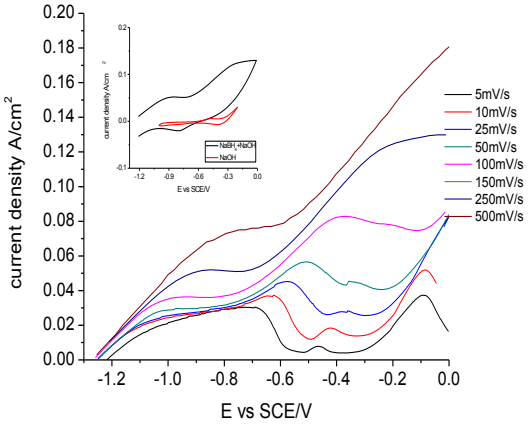

(c)

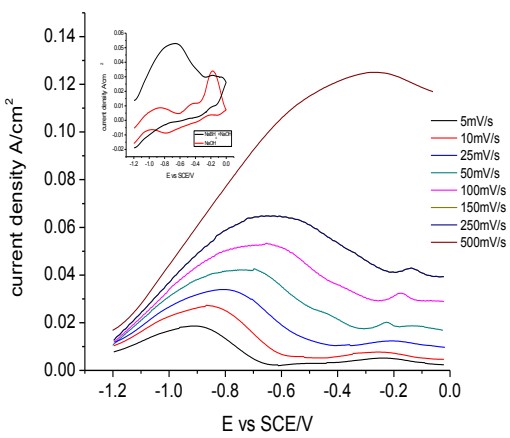

(d)

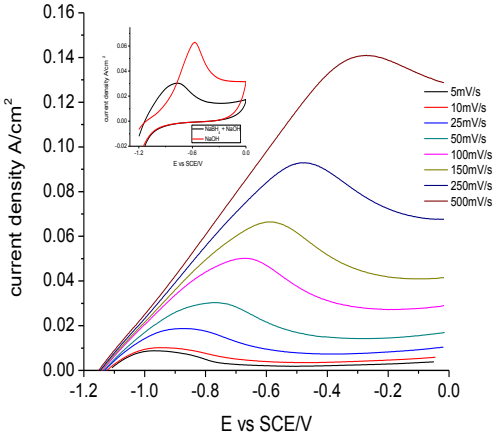

(g)

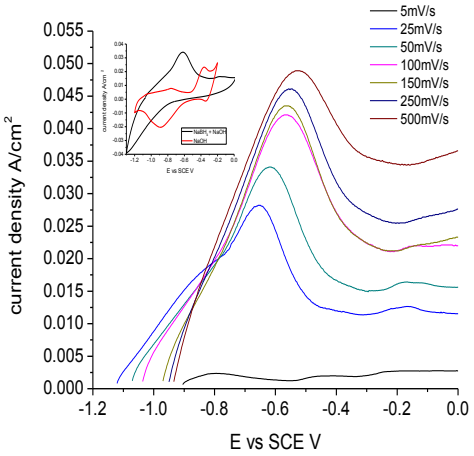

(e)

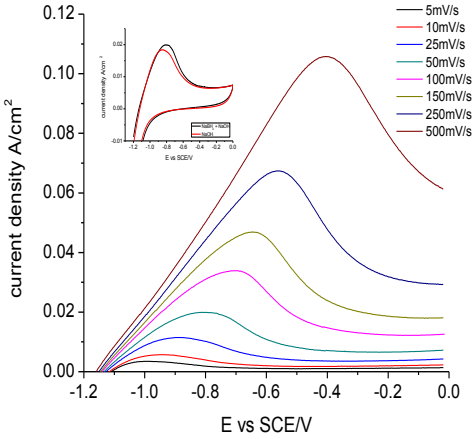

(h)

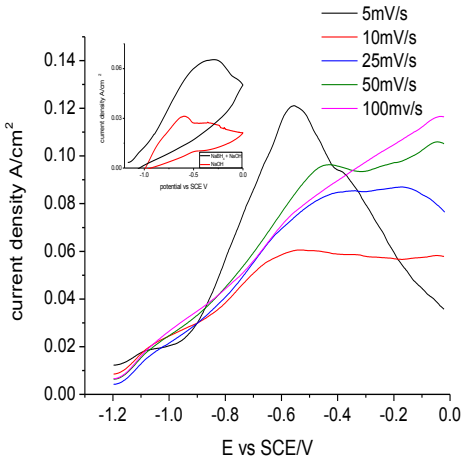

(f)

Figure 2: Voltammograms at different scan rates with insets of control experiment in NaOH at 50 mV.s^{-1}(a) $Ni_{52}Cu_{31}O_{17}$ (b) $Ni_{34}Cu_{37}$ (c) $Ni_{36}Cu_{46}O_{16}$ (d) $Ni_{14}Cu_{26}Fe_{41}O_{18}$ (e) $Ni_4Cu_{48}Fe_{30}O_{12}$ (f) Co_{100} (g) $Ni_{65}Co_{35}$ (h) $Ni_{62}Co_{24}Fe_{14}$.

Table 3: Summary of borohydride oxidation peak analyses.

Foam composition	No. of electron transfer, n	Charge transfer coefficient	Maximum oxidation current density (mA·cm^{-2})	Maximum oxidation Current density per mass of catalyst (mA·g^{-1})
$Ni_{52}Cu_{31}O_{17}$	4.1	0.80	34.3	2882.35
$Ni_{34}Cu_{37}$	12.1	0.91	54.4	3022.22
$Ni_{36}Cu_{46}O_{16}$	12.6	0.87	82.0	9590.64
$Ni_{14}Cu_{26}Fe_{41}O_{18}$	9.8	0.88	124.7	13057.59
$Ni_4Cu_{48}Fe_{30}O_{12}$	1.5	0.71	49.2	28771.93
Co_{100}	-	0.81	97.0	7637.79
$Ni_{65}Co_{35}$	16.1	0.91	140.9	5774.59
$Ni_{62}Co_{24}Fe_{14}$	15.7	0.90	105.9	4394.19

3.4 Hydrogen evolution

The foams were tested for effect of NaOH concentration by conducting the experiment with

different borohydride to NaOH concentrations, for a 4:1 molar ratio of NaOH to $NaBH_4$, Co_{100} foam tended to disintegrate, however all other foams were stable. Results of the hydrolysis experiments are shown in Figure 3. Cobalt and its derivative foams were superior in performance towards hydrolysis of sodium borohydride, which explains the inferior performance in the competing direct electrooxidation of borohydride. Hydrogen evolution rates of up to 30 mL min^{-1} is obtained for pure cobalt foam.

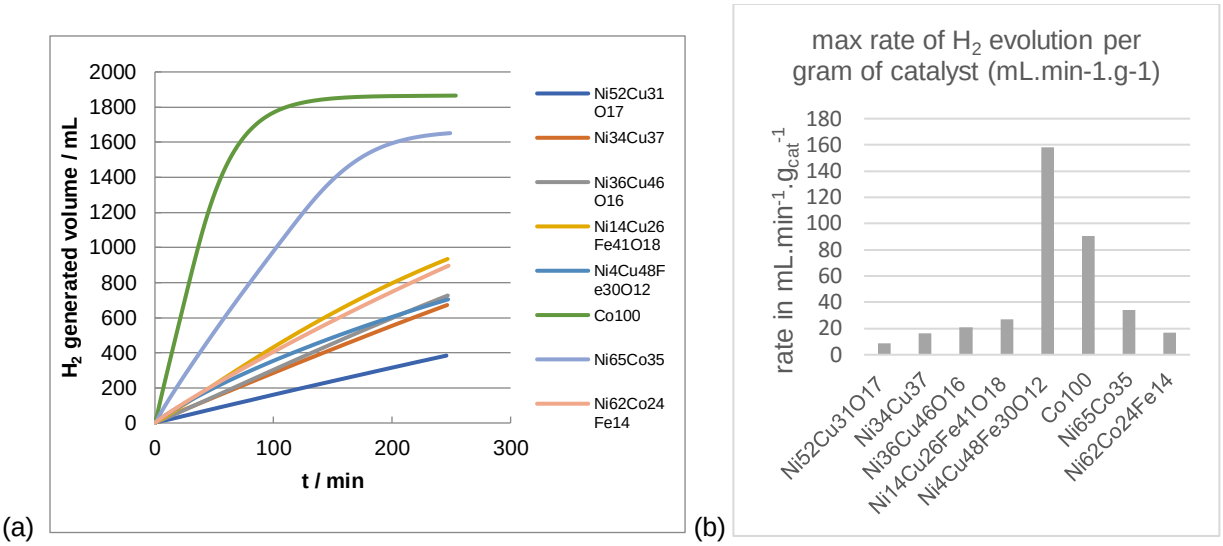

Figure 3: (a) Total volume of hydrogen evolved against time (b) rate of hydrogen evolution per unit gram of catalyst.

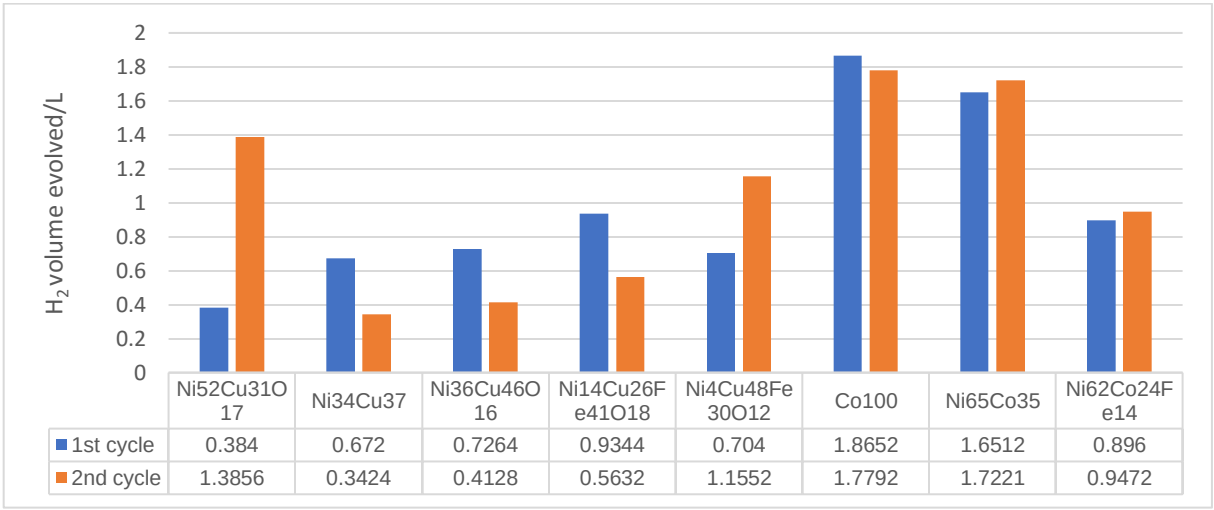

	Ni52Cu31O17	Ni34Cu37	Ni36Cu46O16	Ni14Cu26Fe41O18	Ni4Cu48Fe30O12	Co100	Ni65Co35	Ni62Co24Fe14
1st cycle	0.384	0.672	0.7264	0.9344	0.704	1.8652	1.6512	0.896
2nd cycle	1.3856	0.3424	0.4128	0.5632	1.1552	1.7792	1.7221	0.9472

Figure 4: Activity of foams after two cycles showing total volume of hydrogen evolved during 240 mins.

One would expect loss of activity in the foams through successive cycles as pore spaces and active sites get blocked, however, as shown in Figure 4, a few foams behaved in contrary.

Intermediate oxides which improve the catalytic properties of the foams, formed on the surface of the catalysts, is the most plausible reason for this anomaly.

4 Conclusions

Co-deposition with the hydrogen bubble template presents an easy and efficient method to produce nanoporous three-dimensional metallic foams whose synergistic performances can be optimized towards the exploitation of $NaBH_4$ properties either as a fuel in direct borohydride fuel cells or as a hydrogen carrier for indirect ones. In the case of the former, the presence of cobalt in the catalyst design retards catalytic activity, while it enhances performance in the latter. In terms of foam morphology, the following traits as observed are pivotal to catalyst design; nickel is largely credited for enhancing foam porosity with dendritic pore walls, copper is instrumental to obtain larger apparent pore sizes, iron improved the interconnectivity of the pores, while cobalt favors a 2D architecture-effectively reducing porosity with a characteristic shallowness of surface pores and a densely packed pore wall.

The ternary Ni-Cu-Fe foams presented the best performances towards sodium borohydride oxidation in terms of the current density per unit gram of catalyst, despite a low number of electron transferred in comparison with the binary Ni-Cu foam. Although cobalt foam and its derivative foams had been established as favoring the hydrolysis experiment, the ternary Ni-Cu-Fe foam, outperformed them in terms of rate per unit catalyst weight in the hydrolysis experiment as well.

Cobalt based foams are superior in fast hydrogen demand applications, however, the ternary $Ni_4Cu_{48}Fe_{30}$ foams are the most promising in terms of resource efficiency (mass of catalyst), for both direct and indirect use of sodium borohydride.

References

[1] A. K. Shukla, C. L. Jackson, and K. Scott, “The promise of fuel cell-based automobiles,” *Bull. Mater. Sci.*, vol. 26, no. 2, pp. 207–214, 2003.

[2] J. Larminie and A. Dicks, “Fuel Cell Systems Explained,” *2nd Ed. John Wiley Sons Ltd*, vol. 93, no. 1–2, pp. 14–16, 67–72, 2003.

[3] J. Ma, N. A. Choudhury, and Y. Sahai, “A comprehensive review of direct borohydride fuel cells,” *Renew. Sustain. Energy Rev.*, vol. 14, no. 1. pp. 183–199, 2010.

[4] S. C. Amendola, P. Onnerud, M. T. Kelly, P. J. Petillo, S. L. Sharp-Goldman, and M. Binder, “A novel high power density borohydride-air cell,” *J. Power Sources*, vol. 84, no. 1, pp. 130–133, 1999.

[5] Z. P. Li, B. H. Liu, K. Arai, K. Asaba, and S. Suda, “Evaluation of alkaline borohydride solutions as the fuel for fuel cell,” *J. Power Sources*, vol. 126, no. 1–2, pp. 28–33, 2004.

[6] E. Gyenge, “Electrooxidation of borohydride on platinum and gold electrodes: Implications for direct borohydride fuel cells,” *Electrochim. Acta*,

vol. 49, no. 6, pp. 965–978, 2004.

[7] S. Srinivasan, *Fuel Cells: From Fundamentals to Applications*, vol. 9, no. 10. McGraw Hill Publishing Company New York, NY., 2006.

[8] M. Chatenet, F. Micoud, I. Roche, and E. Chainet, “Kinetics of sodium borohydride direct oxidation and oxygen reduction in sodium hydroxide electrolyte. Part I. BH4\n- electro-oxidation on Au and Ag catalysts,” *Electrochim. Acta*, vol. 51, no. 25, pp. 5459–5467, 2006.

[9] M. H. Atwan, C. L. B. Macdonald, D. O. Northwood, and E. L. Gyenge, “Colloidal Au and Au-alloy catalysts for direct borohydride fuel cells: Electrocatalysis and fuel cell performance,” *J. Power Sources*, vol. 158, no. 1, pp. 36–44, 2006.

[10] B. H. Liu, Z. P. Li, and S. Suda, “A study on performance stability of the passive direct borohydride fuel cell,” *J. Power Sources*, vol. 185, no. 2, pp. 1257–1261, 2008.

[11] D. M. F. Santos, S. Eugénio, D. S. P. Cardoso, B. Šljukić, and M. F. Montemor, “Three-dimensional nanostructured Ni–Cu foams for borohydride oxidation,” *Russ. J. Phys. Chem. A*, vol. 89, no. 13, pp. 2449–2454, 2015.

[12] A. J. Bard and L. R. Faulkner, *Electrochemical methods: fundamentals and applications*, 2nd ed. John Wiley & Sons, Inc., 2001.

[13] “No Title.” [Online]. Available: https://www.chem.uci.edu/~ardo/echem/UCI-CHEM248-2017W_lecture14.pdf. [Accessed: 20-Aug-2017].

[14] B. J. Plowman, L. A. Jones, and S. K. Bhargava, “Building with bubbles: the formation of high surface area honeycomb-like films via hydrogen bubble templated electrodeposition,” *Chem. Commun.*, vol. 51, no. 21, pp. 4331–4346, 2015.

[15] Y. Wang, Y. Shen, K. Qi, Z. Cao, K. Zhang, and S. Wu, “Nanostructured cobalt-phosphorous catalysts for hydrogen generation from hydrolysis of sodium borohydride solution,” *Renew. Energy*, vol. 89, pp. 285–294, 2016.

[16] B. H. Liu, Z. P. Li, and S. Suda, “Nickel- and cobalt-based catalysts for hydrogen generation by hydrolysis of borohydride,” *J. Alloys Compd.*, vol. 415, no. 1–2, pp. 288–293, 2006.

[17] S. Eugénio, U. B. Demirci, T. M. Silva, M. J. Carmezim, and M. F. Montemor, “Copper-cobalt foams as active and stable catalysts for hydrogen release by hydrolysis of sodium borohydride,” *Int. J. Hydrogen Energy*, vol. 41, no. 20, pp. 8438–8448, 2016.

[18] Y. Wei, W. Meng, Y. Wang, Y. Gao, K. Qi, and K. Zhang, “Fast hydrogen generation from NaBH4 hydrolysis catalyzed by nanostructured Co–Ni–B catalysts,” *Int. J. Hydrogen Energy*, vol. 42, no. 9, pp. 6072–6079, 2017.

[19] S. Eugénio, T. M. Silva, M. J. Carmezim, R. G. Duarte, and M. F. Montemor, “Electrodeposition and characterization of nickel--copper metallic foams for application as electrodes for

supercapacitors," *J. Appl. Electrochem.*, vol. 44, no. 4, pp. 455–465, Apr. 2014.

[20] L. Vázquez-Gómez, E. Verlato, S. Cattarin, N. Comisso, P. Guerriero, and M. Musiani, "Electrodeposition of porous Co layers and their conversion to electrocatalysts for methanol oxidation by spontaneous deposition of Pd," *Electrochim. Acta*, vol. 56, no. 5, pp. 2237–2245, 2011.

[21] Santos, D. M F, Šljukić, B., Amaral, L., Milikić, J., Sequeira, C. A C, Macciò, D., Saccone, A., "Nickel-rare earth electrodes for sodium borohydride electrooxidation," *Electrochim. Acta*, vol. 190, pp. 1050–1056, 2016.

[22] B. H. Liu, Z. P. Li, and S. Suda, "Electrocatalysts for the anodic oxidation of borohydrides," *Electrochim. Acta*, vol. 49, no. 19, pp. 3097–3105, 2004.

[23] O. Akdim, R. Chamoun, U. B. Demirci, Y. Zaatar, A. Khoury, and P. Miele, "Anchored cobalt film as stable supported catalyst for hydrolysis of sodium borohydride for chemical hydrogen storage," *Int. J. Hydrogen Energy*, vol. 36, no. 22, pp. 14527–14533, 2011.